Supporting information

Electrostatic-Charge and Electric-Field Induced Smart Gating for Water Transportation

Kai Xiao,[†] Yahong Zhou,[‡] Xiang-Yu Kong,[‡] Ganhua Xie,[†] Pei Li,[†] Zhen Zhang,[†] Liping Wen,[,†] Lei Jiang[*,‡]*

[†] Beijing National Laboratory for Molecular Sciences (BNLMS), Key Laboratory of Green Printing, Institute of Chemistry, Chinese Academy of Sciences, Beijing, 100190, P. R. China

[‡] Key Laboratory of Bioinspired Smart Interfacial Science, Technical Institute of Physics and Chemistry, Chinese Academy of Sciences, Beijing 100190, P. R. China

Table of contents

1. Schematic structure of the experimental setup

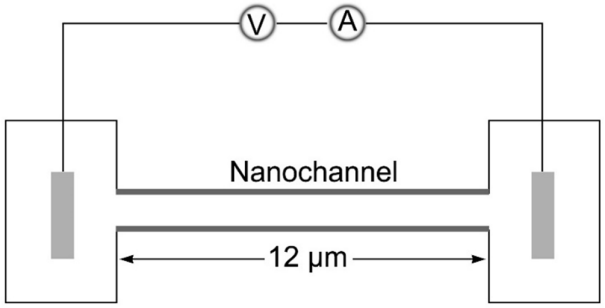

Figure S1. Schematic structure of the experimental setup

The schematic structure of the experimental setup is illustrated in **Figure S1.** In this experiment, a single cylinder-shaped nanochannel was prepared in 12-μm-thick film of polyethylene terephthalate (PET) using a well-developed track-etching technique at 60°C with 2 M NaOH for etching and 1 M KCl + 1 M HCOOH for stopping. The gating was studied by measuring ionic current through the nanochannels. Specifically, a single cylindrical nanochannel PET membrane was mounted between two chambers with 0.1 M electrolyte solution (KCl) and Ag/AgCl electrodes were used to apply a transmembrane potential across the film.[1]

2. Cylindrical nanochannels

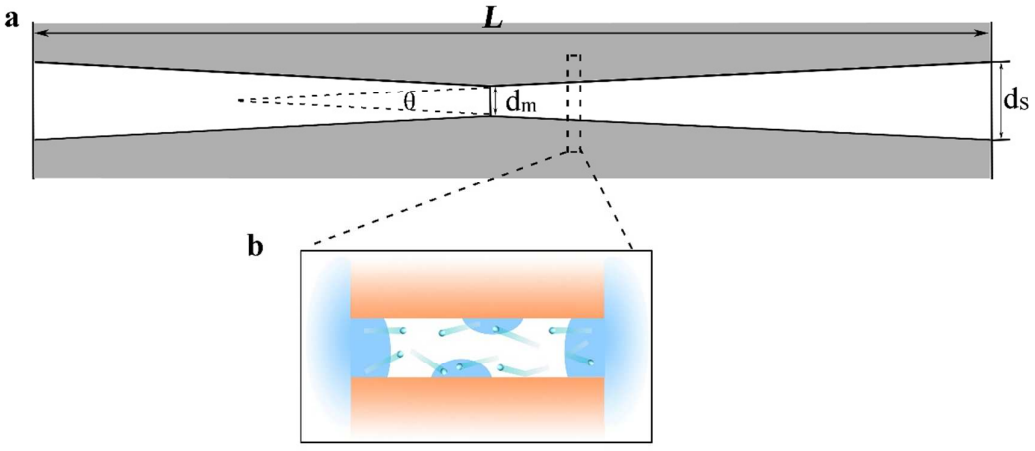

Figure S2. (a) The taper angle of channel is very small. (b) The switch between conduction and non-conduction can be realized in a very short area.

There are two reasons that the channel can be loosely considered as cylindrical.

First, the taper angle of channel is very small. To the surface pore diameter "d_s" and the diameter

in the pore middle "d_m", if the d_s=20 nm, d_m=8 nm, the taper angle can be calculated as:

$$\theta=2\arctan\left[\frac{\frac{d_s-d_m}{2}}{\frac{L}{2}}\right]=2\arctan\left[\frac{\frac{20-8}{2}}{\frac{12000}{2}}\right]=2\arctan\frac{1}{1000}=0.0002$$

This angel is so small that we approximatively consider the channel is cylindrical-shaped (**Figure S2a**).

Second, the wetting and dewetting are always beginning from a patche in the nanochannel, which can act as nucleation sites for the formation of nanoscale gas bubbles. The gas bubbles can extend across the entire nanochannel and disturb the flow of liquid through the nanochannel. It is to say, the switch between conduction and non-conduction can be realized in a very short area, which is in close proximity to cylinder (**Figure S2b**).

3. Geometrical parameters and statistical of the cylindrical nanochannels

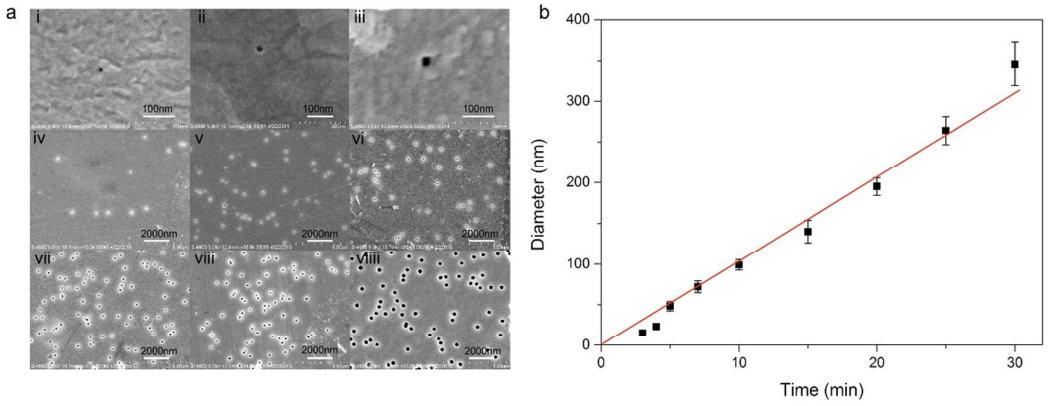

Figure S3. (a) SEM image of the nanochannels under different etching time (i to viii). **(b)** The statistical result of the channel diameter. A very good linear relationship between etching time and pore diameter is found.

Geometrical parameters of the nanochannels were studied and analyzed from multichannel membranes (density of $1\times10^8/cm^2$) prepared under the same condition as single cylindrical nanochannel used in this experiment. SEM was used to get the diameters of the cylindrical multichannels, which were taken in the field-emission mode using a Hitachi S-4800 microscope at an accelerating voltage of 5 kV. Statistical results over 100 measurements from 10 membranes for each data point show a very good linear relationship between the pore diameter and the etching time (**Figure S3**). The calculated bulk etching rate is 5.5±0.2 nm/min, which is similar to Nguyen et al's

and Liu et al's report.[2]

4. The stability of electrostatic induced gating

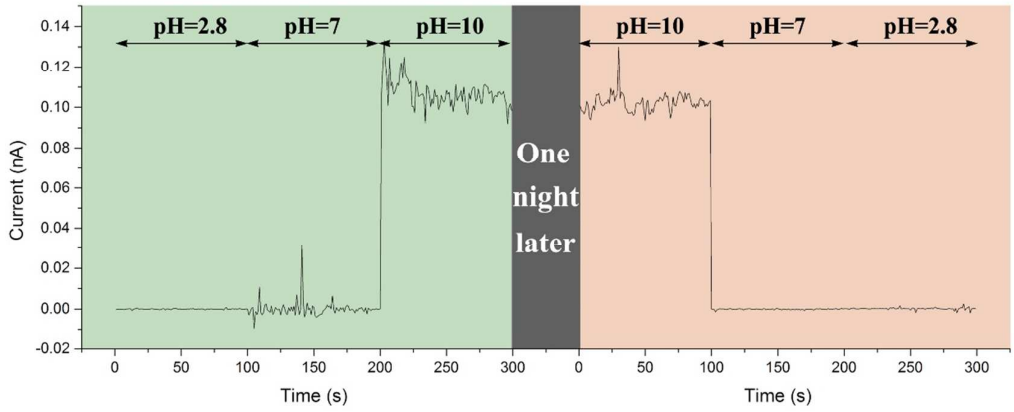

Figure S4. The stability of electrostatic induced gating. After immersed in electrolyte solution of pH 10 for one night, the gating maintained steady current of conductive state under pH 10 while stated in non-conductive state under pH 7 and 2.8.

In this experiment, single nanochannels were prepared in 12-μm-thick films of polyethylene terephthalate (PET) using a well-developed track-etching technique at 60°C with 2 M NaOH. To confirm this gating is stable in alkaline electrolyte solutions, we immersed the nanochannel with diameter ~7nm in electrolyte solution of pH 10 for one night. This nanochannel is non-conductive under pH 3 and 7 while conductive with ~100 pA under pH 10. After been immersed in electrolyte solution of pH 10 for one night, this phenomenon is not changed, which can prove our system is stable in alkaline electrolyte solutions.

5. Gating characterized by current-voltage curves

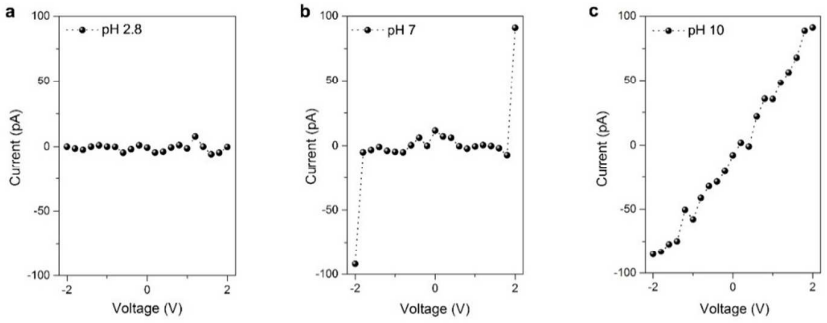

Figure S5. Current-Voltage curves under varied electrolyte solution (pH=2.8, 7, 10).

Current-voltage curves in **Figure S5 a** showed that the gating was closed completely under pH

2.8 in measured voltages ranging from -2 V to 2 V. If the electrolyte was regulated to pH 7, this gating was closed under low bias voltage while opened abruptly at ± 2 V (**Figure S5 b)**. Under pH 10, a symmetric ionic current as other symmetric nanochannels obtained due to the introduced high density negative charges (**Figure S5 c)**, which verified that electrostatic charges played important roles in regulating gating properties.

6. Statistic conduction of the gating

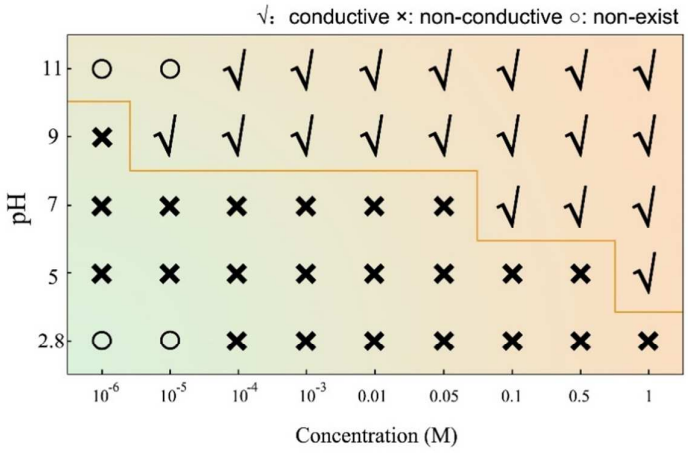

Figure S6. The statistic conduction of the smart gating. The gating is open under the cooperative conditions of high pH value and high electrolyte solution concentration while close under the cooperative conditions of low pH value and low electrolyte solution concentration. The diameter of nanochannel is approximately 7 nm.

The statistic conduction of the gating with diameter ~7 nm was performed under the pH scope from 2.8 to 11 and the KCl concentration scope from 10^{-6} M to 1 M (**Figure S6)**. Generally, the gating was opened under the cooperative conditions of high pH value and concentrated electrolyte while closed under the cooperative conditions of low pH value and dilute electrolyte. Specifically, the conductive and non-conductive states of the nanochannel depend on the electrolyte concentration under pH 5, 7, and 9. These results could be explained by the distributions of the osmotic and the Maxwell stress, which were caused by interaction of the channel surface charges induced by regulating electrolyte pH and counter-ions in the electrolyte.[3] Especially, the gating was always conductive under pH 11 while non-conductive under pH 2.8 no matter what concentration electrolyte was used, indicating that the single sub-10-nm channel exhibit surface charge dependent transport properties.

7. The threshold voltage between conductive and non-conductive

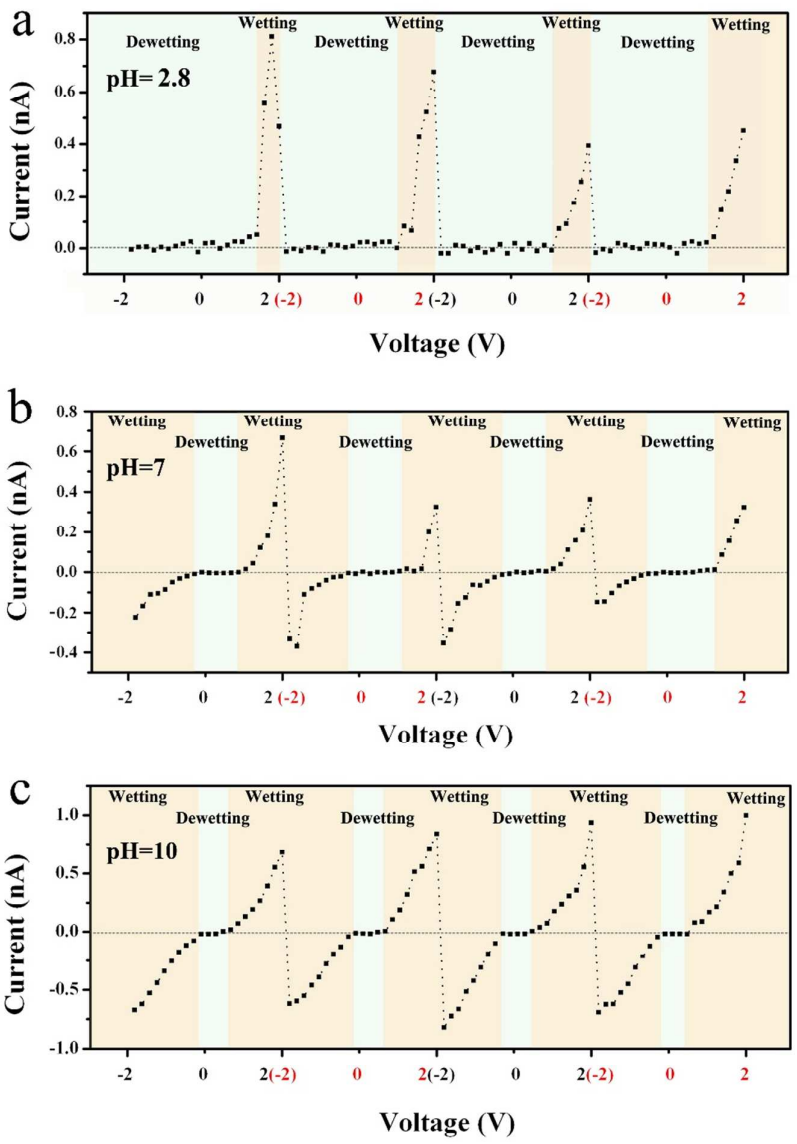

Figure S7. The threshold voltage between conductive and non-conductive (transition point) is different at varied pH (pH 2.8, 7, 10). Current-Voltage characteristic obtained by four cycles with the voltage changed in steps of 0.2 v from -2 v to +2 v at pH 2.8 **(a)**, 7 **(b)**, 10 **(c)**. For pH 2.8, the nanochannel stayed in deweetting (non-conductive) states for almost all the cycle **(a)**. The threshold voltage decreased from about 2 V to about 0.8 V (**b** pH=7) and 0.2 V (**c** pH=10).

The threshold voltage between conductive and non-conductive (transition point) is different under varied pH values. Under pH 2.8 **(Figure S7 a)**, the nanochannel stayed in dewetting (non-conductive) states for almost all the cycles and only can be wetted in high voltage (2 V). Under pH 7 **(Figure S7**

b), the threshold voltage from non-conductive to conductive decreased from about 2 V to about 0.8 V due to the introducing of low density surface charge. Under pH 10 **(Figure S7 c)**, the threshold voltage from non-conductive to conductive decreased to about 0.2 V due to the introducing of high density surface charge. This phenomenon indicated that the wetting and dewetting of the nanochannel was closely related with the surface charge.

8. Typical examples of gate induced by voltage under varied pH

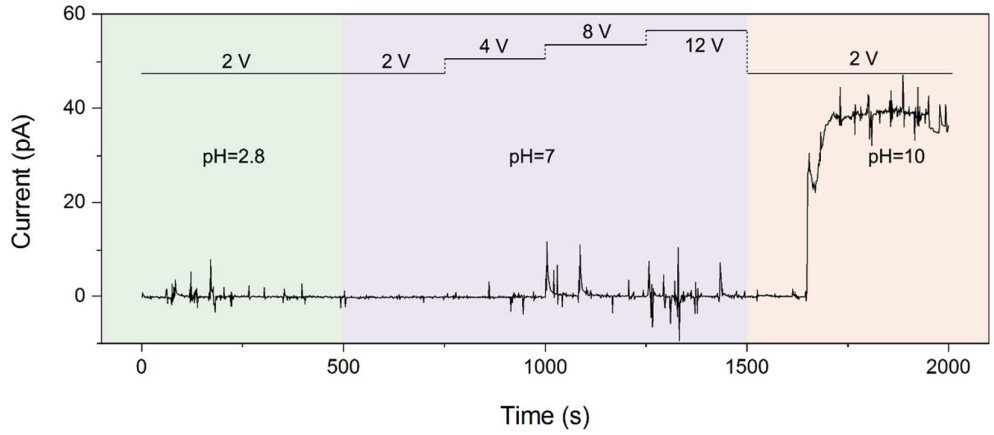

Figure S8. Typical examples of voltage-induced gate under varied pH. Under pH 2.8 and 7, the nanochannel cannot be infiltrated even at high external voltage (12 V) while the nanochannel is full negative charged and conductive at low external voltage (2 V).

The gating can be regulated by external voltage with the cooperation of surface charge. Under pH 2.8 and 7, the nanochannel cannot be infiltrated even at high external voltage (12 V) while the nanochannel is fully negatively charged and conductive at low external voltage (2 V). This result indicated that the surface charge played the most important role while voltage had a secondary effect in the gating from conductive and non-conductive.

9. The influence of diameter

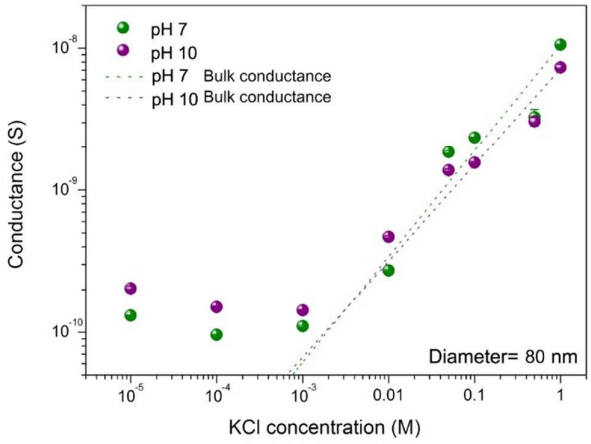

Figure S9. Both the ionic conductance under pH 7 (green ball) and 10 (purple ball) deviates from bulk value (green and purple dashed line) from below ~0.001 M, which indicate that the ion transport of the nanocahnnel with diameter 50 nm is not goverend by surface charge.

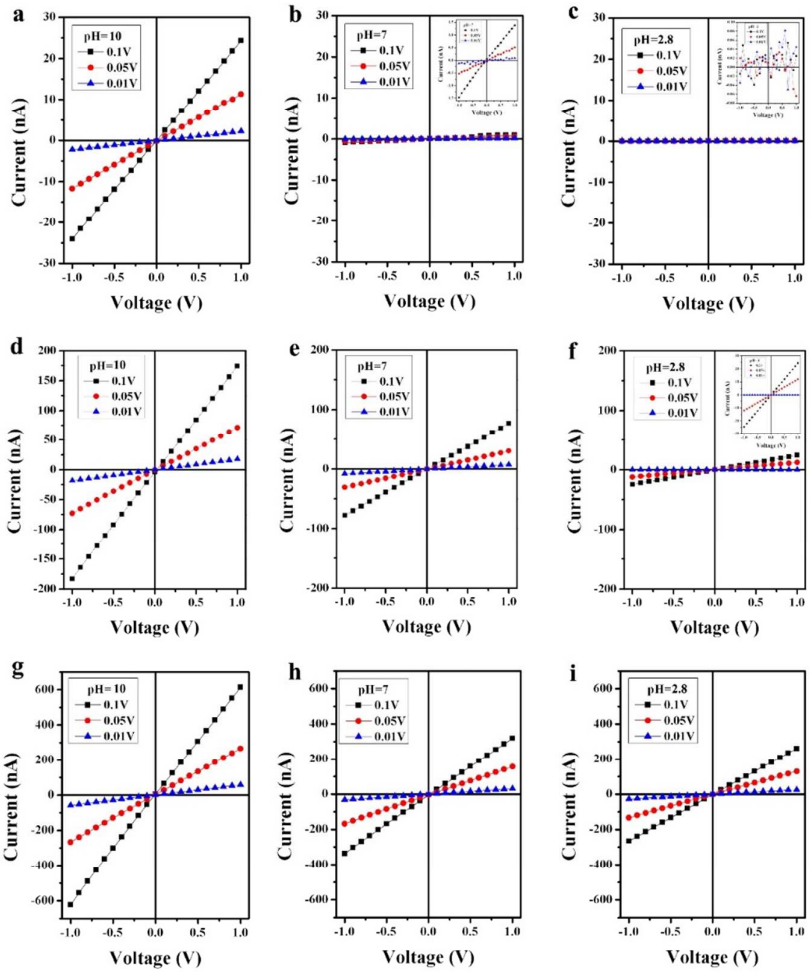

Figure S10. Current voltage curves through cylindrical nanochannels ($1\times10^8/cm^2$). (a-c) Current voltage curves of

nanochannels with diameter ~5nm under varied pH (2.8, 7, 10). **(d-f)** Current voltage curves of nanochannels with diameter ~10nm under varied pH (2.8, 7, 10). **(g-i)** Current voltage curves of nanochannels with diameter ~20nm under varied pH (2.8, 7, 10).

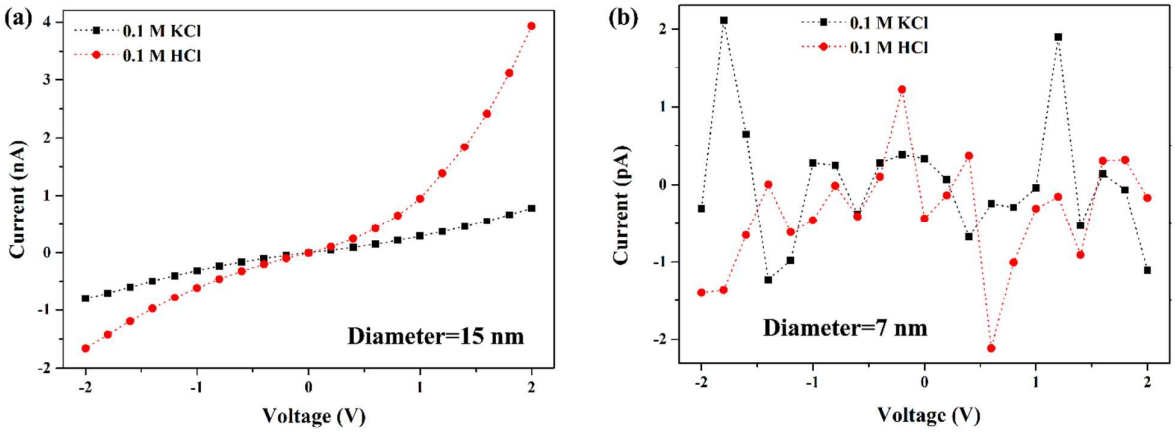

Figure S11. Hydrochloric acid transport through PET nanochannels with different diameters.

To the nanochannel of diameter ~80 nm (**Figure S9**), the conductance measured with pH 7 and pH 10 had no obvious difference whether in the high KCl concentration or low KCl concentration, since the diameter was far from the double layer overlap regime.[4]

The cylindrical nanochannels also exhibited electrostatic induced voltage-gating properties. To the nanochannel with diameter ~5nm, the nanochannel was conductive under pH 7 and 10 with step current along with step voltage **(Figure S10 a,b)** while non-conductive under pH 2.8 regardless of the voltage **(Figure S10 c)**. To the nanochannel with diameter ~10nm, similar conductive state could be obtained under pH 7 and 10 **(Figure S110 d,e)** as well as under the high voltage of pH 2.8 while non-conductive under 0.01 V of pH 2.8 **(Figure S10 f blue line)**. To the nanochannel with diameter ~20nm, conductive states with step current **(Figure S10 g-i)** could be observed under varied pH values.

We measured the ionic current in nanochannels with diameter 15 nm and 7nm. The hydrochloric acid can pass through PET nanochannels with 15 nm diameter (**Figure S11 a)** while cannot pass through the channel with 5 nm diameter (**Figure S11 b)**, which indicated that there are nanobubbles in the channel.

10. Contact angles of the planar PET films under varied pH

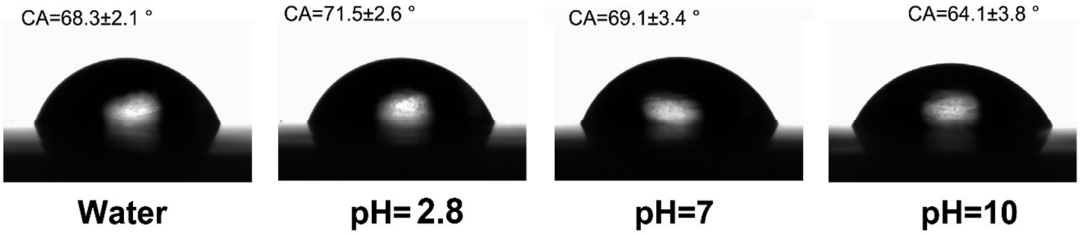

Figure S12. Contact angles of the planar PET films. The contact angles have no obvious difference under varied electrolyte solution.

Contact angles were measured using an OCA20 (DataPhysics, Germany) contact-angle system at ambient temperature and saturated humidity. The planar PET membrane was prepared under the same condition as single cylindrical nanochannel membrane. The water droplet is 2 μL and the measurement was in five different locations of the membrane. As shown in **Figure S12**, the contact angle was about 71 ° under pH 2.8 while decreased to about 64 ° under pH 10, which was result from the change of surface charge.

11. The difference of contact angle on horizontal surface and concave surface

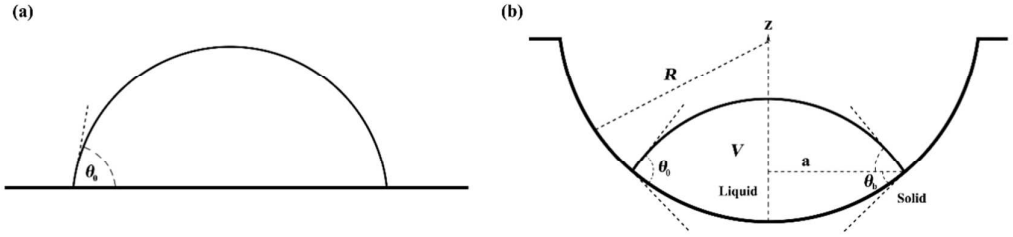

Figure S13. Illustrations of small, sessile liquid drops of volume V on various types of surfaces. (a) on a flat, horizontal surface, (b) inside of a hemispherical cavity.

Usually, a small drop is gently deposited on a horizontal solid surface. A small amount of liquid may be added to or withdrawn from the drop to advance or retract its contact line; then, a contact angle, depicted in **Figure S13a**, is measured. However, there are many scenarios where it is desirable to measure wettability of more complex surfaces.[5-9] Surfaces that are rough may hamper establishment of a well-defined baseline. (**Figure S13b**) For example, if the drop is sufficiently small

that no gravitational distortion occurs such that the drop has the proportions of a spherical segment, θ_0 can be estimated from the base diameter (2a) and drop volume (V)

$$\theta_0=2\cdot\arctan\left(\frac{\left(\frac{48V}{\pi(2a)^3}+\left(4+\left(\frac{48V}{\pi(2a)^3}\right)^2\right)^{1/2}\right)^{2/3}-2^{2/3}}{2^{1/3}\left(\frac{48V}{\pi(2a)^3}+\left(4+\left(\frac{48V}{\pi(2a)^3}\right)^2\right)^{1/2}\right)^{1/3}}\right) \quad \text{Eq.1}$$

As before, assume that the drop is symmetrically centered, is not distorted by gravity, and has spread to produce an intrinsic contact angle, θ_0. The analysis of the concave case differs from that of the convex case in two aspects. First, the intrinsic contact angle (θ_0) is the sum of the apparent value (θ) and the curvature angle (θ_b)

$$\theta_0=\theta+\theta_b \quad \text{Eq.2}$$

Second, the apparent drop volume on the concave surface (Vc) is less than V

$$V_c=V-V_b \quad \text{Eq.3}$$

By following the approach given above, we arrive at an expression that allows for indirect contact angle estimation on concave surfaces in terms of dimensions and volume

$$\theta_0=2\cdot\arctan\left(\frac{\left(\frac{48V_c}{\pi(2a)^3}+\left(4+\left(\frac{48V_c}{\pi(2a)^3}\right)^2\right)^{1/2}\right)^{2/3}-2^{2/3}}{2^{1/3}\left(\frac{48V_c}{\pi(2a)^3}+\left(4+\left(\frac{48V_c}{\pi(2a)^3}\right)^2\right)^{1/2}\right)^{1/3}}\right)+\arcsin\left(\frac{2a}{2R}\right) \quad \text{Eq.4}$$

Where

$$V_c=V-\frac{1}{3}\pi\cdot R^3\left(2-3\left(1-\left(\frac{2a}{2R}\right)^2\right)^{1/2}+\left(1-\left(\frac{2a}{2R}\right)^2\right)^{3/2}\right) \quad \text{Eq.5}$$

We assume R=5 nm a=2.5 nm V=20 nL. We can get the Vc about 13.27 nL from eq5. The calculated contact angle on horizontal surface is approximately 70 ° while the contact angle on concave surface is approximately 83 °. If we assume R=3 nm, a=1.5 nm, V=4 nL, we can get the Vc about 3.55 nL from Eq.5. The calculated contact angle on horizontal surface is approximately 76 ° while the contact

angle on concave surface is approximately 92 °. Thus, the wetting and dewetting of electrostatic inducing voltage-gating can be realized in a single sub-10-nm cylindrical nanochannel with planar contact angle of ~65°.

12. Reference

[1] a) P. Y. Apel, I. V. Blonskaya, O. L. Orelovitch, P. Ramirez, B. A. Sartowska, *Nanotechnology* **2011**, *22*, 175302; b) P. Y. Apel, I. Blonskaya, O. Orelovitch, S. Dmitriev, *Nuclear Nucl. Instrum. Meth. B* **2009**, *267*, 1023-1027.

[2] a) N. Liu, Y. Jiang, Y. Zhou, F. Xia, W. Guo, L. Jiang, *Angew. Chem. Int. Ed.* **2013**, *52*, 2007-2011; b) Q. H. Nguyen, M. Ali, V. Bayer, R. Neumann, W. Ensinger, *Nanotechnology* **2010**, *21*, 365701.

[3] a) J. A. Lee, I. S. Kang, *Phys. Rev. E* **2014**, *90*, 032401; b) L. Innes, D. Gutierrez, W. Mann, S. F. Buchsbaum, Z. S. Siwy, *Analyst* **2015**, **140**, 4804-4812,

[4] a) L. Onsager, N. N. T. Samaras, *J. Chem. Phys.* **1934**, *2*, 9; b) C. W. Outhwaite, *Chem. Phys. Lett.* **1970**, *5*, 77-79.

[5] Shin, J. Y. & Abbott, N. L. Using light to control dynamic surface tensions of aqueous solutions of water soluble surfactants. *Langmuir* **15**, 4404-4410, (1999).

[6] Extrand, C. W. & Moon, S. I. Indirect methods to measure wetting and contact angles on spherical convex and concave surfaces. *Langmuir.* **28**, 7775-7779, (2012).

[7] Wang, Y. & Zhao, Y.-P. Electrowetting on curved surfaces. *Soft Matter* **8**, 2599, (2012).

[8] Dzubiella, J. & Hansen, J. P. Electric-field-controlled water and ion permeation of a hydrophobic nanopore. *J. Chem. Phys.* **122**, 234706, (2005).

[9] Li, J. *et al.* Electrostatic gating of a nanometer water channel. *Proc. Natl. Acad. Sci. USA* **104**, 3687-3692 (2007).